No evidence of nanodiamonds in Younger–Dryas sediments to support an impact event

Tyrone L. Daulton[a,1], Nicholas Pinter[b], and Andrew C. Scott[c]

[a]Department of Physics and Center for Materials Innovation, Washington University in St. Louis, St. Louis, MO 63130; [b]Department of Geology, Southern Illinois University, Carbondale, IL 62901; and [c]Department of Earth Sciences, Royal Holloway University of London, Egham, Surrey TW20 OEX, United Kingdom

Edited by Mark H. Thiemens, University of California at San Diego, La Jolla, CA, and approved July 27, 2010 (received for review March 24, 2010)

The causes of the late Pleistocene megafaunal extinctions in North America, disappearance of Clovis paleoindian lithic technology, and abrupt Younger–Dryas (YD) climate reversal of the last deglacial warming in the Northern Hemisphere remain an enigma. A controversial hypothesis proposes that one or more cometary airbursts/impacts barraged North America ≈12,900 cal yr B.P. and caused these events. Most evidence supporting this hypothesis has been discredited except for reports of nanodiamonds (including the rare hexagonal polytype) in Bølling–Ållerod-YD-boundary sediments. The hexagonal polytype of diamond, lonsdaleite, is of particular interest because it is often associated with shock pressures related to impacts where it has been found to occur naturally. Unfortunately, previous reports of YD-boundary nanodiamonds have left many unanswered questions regarding the nature and occurrence of the nanodiamonds. Therefore, we examined carbon-rich materials isolated from sediments dated 15,818 cal yr B.P. to present (including the Bølling–Ållerod-YD boundary). No nanodiamonds were found in our study. Instead, graphene- and graphene/graphane-oxide aggregates are ubiquitous in all specimens examined. We demonstrate that previous studies misidentified graphene/graphane-oxide aggregates as hexagonal diamond and likely misidentified graphene as cubic diamond. Our results cast doubt upon one of the last widely discussed pieces of evidence supporting the YD impact hypothesis.

archaeology | paleoclimate | Quaternary extinctions | carbon spherules | fungal sclerotia

During the end of the last glacial period in the Northern Hemisphere near 12,900 cal yr B.P., deglacial warming of the Bølling–Ållerod interstadial ceased abruptly (1) and glacial conditions were restored for a ≈1,300-yr interval known as the Younger–Dryas (YD) stadial (2–5). Conclusion of the YD was abrupt with temperature increasing to present-day Holocene-interglacial levels within a few decades (2, 6). In North America at least 17 genera of megafauna (e.g., mammoths, mastodons, giant short-faced bears, saber-tooth tigers, and numerous other megafauna species) became extinct near the YD onset, although the details of the chronology are in question (7, 8). North America's earliest known human populations arrived and dispersed prior to the YD, and their Clovis lithic technology disappeared from the sedimentary record near the onset of the YD (9, 10). Although the YD climate reversal as well as the geologically abrupt Pleistocene megafauna extinctions and disappearance of the Clovis culture are not disputed, their causes are matters of intense debate.

Most paleoclimatologists believe the YD stadial resulted when a massive volume (~9,500 km^3) of fresh water from the proglacial Lake Agassiz released into the northern Atlantic and disabled the thermohaline circulation (4, 11). However, the YD has also been attributed to cessation in the El Niño Southern oscillation caused by changes in Earth's orbital configuration (12). Although climate change undoubtedly applied stress to the megafauna and human populations, it remains unclear if that alone was sufficient to catastrophically impact animal populations. Widespread hunting of megafauna by Clovis paleoindians and disease have also been proposed.

A recent hypothesis suggests that an extraterrestrial body, either a fragmented chondritic meteorite or comet, detonated as airburst(s) and/or impact(s) over North America, igniting continent-wide wildfires and injecting a large mass of dust into the atmosphere (13–16). The energy deposited by the bolides is speculated to have induced partial melting of the Laurentide ice sheet, disabling the North Atlantic thermohaline circulation and initiating the YD stadial. The combined environment impact would have adversely affected animal populations. In numerous sites throughout North America, the Bølling–Ållerod-YD sedimentary boundary is characterized by a black organic-containing layer (often termed "black mat") (9, 17), whose base is near the boundary and is interpreted by impact proponents as a hemisphere-wide deposit from wildfires (13–16). Elevated concentrations (with respect to overlying and underlying sediments) of impact markers are reported in YD black mats from 10 Clovis-age archaeological sites and 15 Carolina bays on the Atlantic Coastal Plain: specifically, iridium, nickel, magnetic microspherules, fullerenes enriched in trapped ^{3}He, charcoal/soot, carbon spherules, glass-like carbon, and nanodiamonds (13–16). Among these reported markers is the rare hexagonal (2H) polytype of diamond, lonsdaleite (16). Lonsdaleite is often associated with shock pressures related to impacts where it has been found to occur naturally; see refs. 18–21. Many of the impact markers reported in YD black mats have been widely discredited (22–27) with the exception of the enigmatic nanodiamonds.

Results and Discussion

To investigate the presence and nature of Bølling–Ållerod-YD-boundary nanodiamonds, we microcharacterized the carbon allotropes in carbonaceous materials from the base of YD black mats and other dated sources using transmission electron microscopy (TEM). The carbonaceous phases in carbon spherules and microcharcoal isolated from YD black mats are identical to those in spherules and glassy carbon isolated from older sediments as well as obtained from a modern forest fire. All specimens were predominantly C and contained the same dominant minerals: amorphous carbon (a-C), graphene, graphene/graphane, and graphite (all but the former displaying varying degrees of disorder). Neither cubic nor hexagonal diamond was identified in any of the samples. Trace amounts of submicrometer to nanometer-sized minerals were observed, including Fe and Cu oxides as well as Ti-, Si-, and/or Ca-rich grains.

The dominant crystalline carbonaceous phase in carbon spherules, microcharcoal, and glassy carbon was graphene in the form

Author contributions: T.L.D., N.P., and A.C.S. designed research, performed research, analyzed data, and wrote the paper.

The authors declare no conflict of interest.

This article is a PNAS Direct Submission.

[1]To whom correspondence should be addressed. E-mail: tdaulton@physics.wustl.edu.

This article contains supporting information online at www.pnas.org/lookup/suppl/doi:10.1073/pnas.1003904107/-/DCSupplemental.

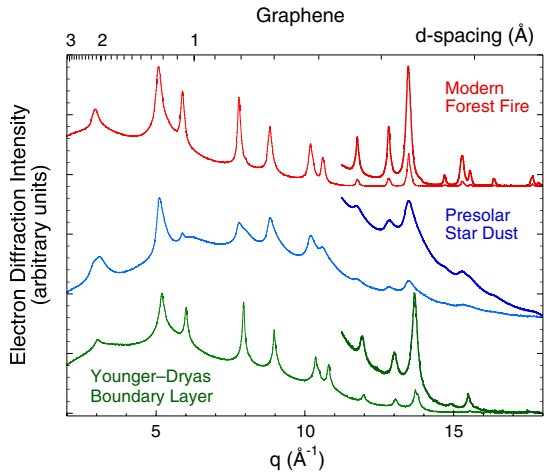

Fig. 1. Radial mean of electron diffraction intensity for graphene (thin lines) of modern origin (charred fungal Sclerotium), of supernova origin [cores of graphitic spherules isolated from the carbonaceous chondrite meteorite Murchison (30)], and from the onset of the Younger–Dryas (carbon spherules isolated from Santa Rosa Island, CA). Diffraction patterns were also acquired with longer exposure times to measure faint, high-angle peaks (thick lines). Graphene in microcharcoal from Murray Springs, AZ (~12,900 cal yr B.P.) and in carbon spherules as well as glassy carbon from Santa Cruz Island, CA (15,498–16,209 cal yr B.P.) are nearly identical to above.

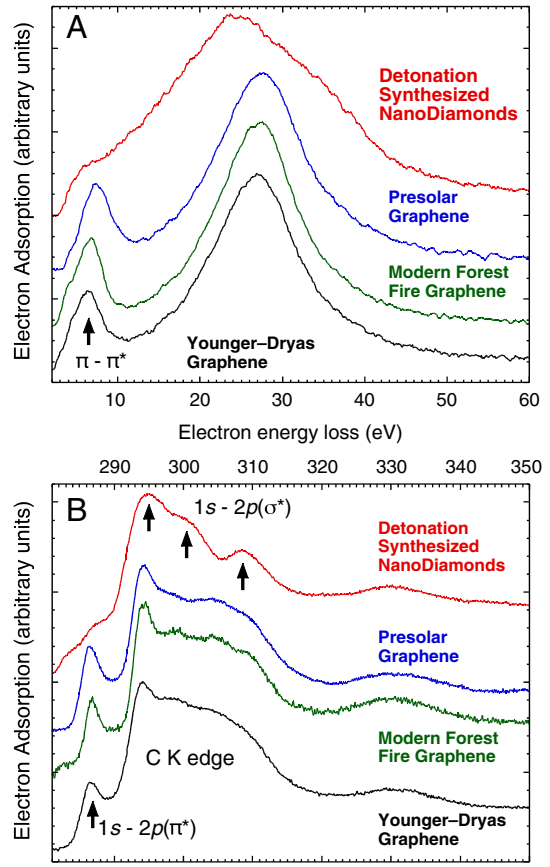

Fig. 2. Comparison of low-loss (*A*) and core-loss (*B*) electron energy loss spectra acquired from specimens overhanging holes in the support film (EELS collection half angle $2\beta = 6.34 \pm 0.06$ mrad). Shown are detonation synthesized nanodiamonds as well as graphene of supernova origin [Murchison meteorite (30)], of modern origin (charred fungal Sclerotium), and from the onset of the Younger–Dryas (Santa Rosa Island, CA). See Fig. 1 caption for expanded details. Arrows indicate peaks associated with π-π^* and 1*s*-2$p(\pi^*)$ sp^2 graphitic transitions as well as 1*s*-2$p(\sigma^*)$ sp^3 diamond transitions.

of polycrystalline aggregates (Figs. 1–3 and Table 1). Graphene is a two-dimensional, single-atom-thick planar molecule with sp^2-bonded carbon (1.42 ± 0.1 Å bond length) in a hexagonal arrangement of 2.46 ± 0.02 Å edge length (28, 29). In the form of a polycrystalline aggregate, as first observed in the cores of many circumstellar graphite spherules isolated from chondritic meteorites (30), graphene sheets are randomly oriented and lack any correlation. When periodically stacked normal to their plane (e.g., *AB*, *AA*, or *ABC* stacking), graphene sheets form various graphite polytype structures or turbostratic graphite if the stacking is disordered.

Core-loss absorption edges were measured using TEM electron energy loss spectroscopy (EELS) to determine the elements present, quantify their concentration, and characterize their local bonding. Elemental maps acquired using EELS spectrum imaging of core-loss edges demonstrate that terrestrial graphene aggregates contain predominantly C, but also heterogeneous distributions of O at upward of ≈6 at. % indicating partial and inhomogeneous oxidation. Discrete tens-of-nanometer diameter Ca- and O-rich grains were sometimes observed embedded within graphene aggregates. The near-edge structure of EELS core-loss spectra is highly dependent on the local bonding of an element and is sensitive to valence, crystal field splitting (e.g., atom coordination and low- or high-spin configurations), spin-orbit interactions, atomic Coulomb repulsion, and exchange effects. Low-loss EELS spectra are also dependent on local bonding. Further confirming the grains identified as (sp^2-bonded) graphene are not diamond, both the low- and core-loss EELS spectra of graphene are distinct from that of sp^3-bonded diamond (Fig. 2).

For all specimens examined, some graphene aggregates exhibited diffraction lines that were asymmetric (indicative of texturing) and doubled (Figs. 3 and 4). The extra set of reflections showed varying degrees of diffuseness (i.e., disorder). For some aggregates, their second set of reflections could be isolated from

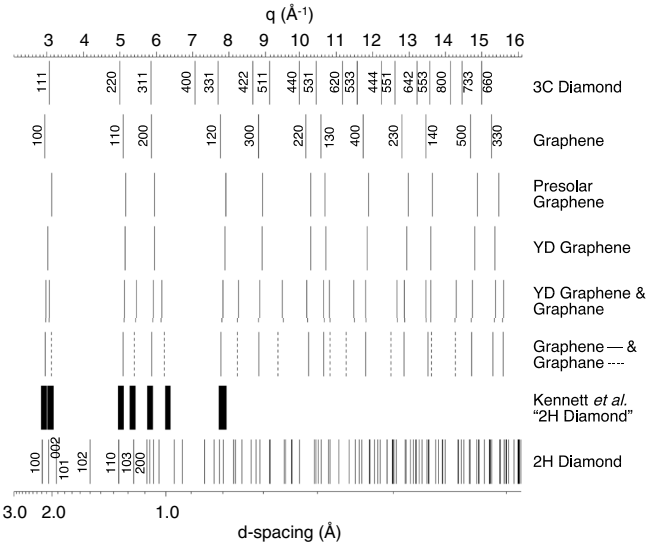

Fig. 3. Electron diffraction peaks calculated for 3C cubic diamond, 2H hexagonal diamond, graphene, and graphene/graphane mixture compared to those measured from presolar graphene as well as graphene and graphene/graphane aggregates in carbon spherules isolated from Santa Rosa Island, CA. In the electron diffraction patterns identified as hexagonal diamond by Kennett et al. (16), asymmetrically doubled diffraction lines are clearly evident in their Fig. S2*B* as well as discernible in both their Fig. 2*F* and Fig. S2*A*. Peaks measured from the doubled diffraction lines in Fig. S2*B* of Kennett et al. (16) are shown (we calibrated the reported {100} reflection to 2.189 Å, and the line widths represent the error in our measurement). Kennett et al. (16) identified their Fig. S2*C* as hexagonal diamond; however, it is also consistent with diffraction normal to the graphite basal plane; graphite {100} (2.139 Å) is close to that of lonsdaleite {100} (2.182 Å).

Table 1. Electron diffraction planar spacings

3C Diamond		Graphene/graphane—oxide					
Indices	Calculated, Å	Indices	Calculated graphene, Å	Presolar graphene, Å*	Younger–Dryas graphene, Å*,†	Younger–Dryas graphane, Å*,†,‡	Calculated graphane, Å
111	2.053	100	2.130	2.033 (6)	2.076 (4)	2.004 (7)	2.021
220	1.257	110	1.230	1.230 (2)	1.222 (2)	1.158 (2)	1.167
311	1.072	200	1.065	1.069 (3)	1.061 (2)	0.991 (3)	1.010
400	0.889						
331	0.816	120	0.805	0.807 (2)	0.798 (1)	0.754 (2)	0.764
422	0.726	300	0.710	0.709 (2)	0.705 (1)	0.657 (1)	0.674
511/333	0.684						
440	0.629	220	0.615	0.616 (1)	0.609 (1)	0.575 (2)	0.583
531	0.601	130	0.591	0.593 (1)	0.584 (1)	0.547 (5)	0.561
620	0.562						
533	0.542	400	0.533	0.534 (1)	0.525 (1)	0.496 (2)	0.506
444	0.513						
551/711	0.498	230	0.489	0.489 (1)	0.479 (1)	0.460 (1)	0.464
642	0.475						
553/731	0.463	140	0.465	0.465 (1)	0.455 (1)	0.436 (6)	0.441
800	0.445						
733	0.434	500	0.426	0.427 (1)	0.418 (1)	0.400 (1)	0.404
660/822	0.419	330	0.410	0.410 (1)	0.397 (1)	0.381 (1)	0.389

*Detonation synthesized nanodiamonds were used to calibrate diffraction camera length of microscope. Values in parentheses are the measurement error (in the least significant digit) based on standard error of replicate measurements and the error in camera length calibration (±0.2%).
†Hexagonal edge length varies slightly from grain to grain.
‡Measured from graphene/graphane aggregates.

the first using a small selected-area aperture (Fig. 4), and EELS showed those regions were also predominantly C with varying O concentrations, demonstrating the presence of a modified form of graphene. The modified graphene exhibited a $5.1 \pm 0.3\%$ (see Table 1) contraction in hexagonal edge length, although the contraction varied somewhat from aggregate to aggregate. This is consistent with the previously theorized but only recently synthesized hydrogenated form of graphene, termed graphane (29), which exhibits a 5% reduction in edge length resulting from buckling of C bonds out of the plane of the C sheet due to H bonding on sheet faces. The third-most abundant crystalline carbonaceous phase was graphite with various degrees of graphene-sheet stacking disorder.

Careful analysis must be exercised in identifying diamond polytypes in carbonaceous specimens. Graphene diffraction lines closely resemble those of cubic diamond for small Bragg angle (Fig. 3 and Table 1). The first five diffraction spacings of graphene approximately mirror those of cubic diamond with the notable exception that graphene lacks analogous diffraction intensity to that from {400} diamond planes. Differences between the two structures become more pronounced at larger Bragg angles. It is possible that graphene aggregates, which are ubiquitous in carbon spherules, microcharcoal and glassy carbon, were misidentified as cubic diamond in previous studies of the YD-boundary deposits (13, 15, 16) because no {400} reflections (or EELS spectra) were reported and diffraction lines were measured only over a small range of Bragg angles (15, 16).

Also reported in YD-boundary deposits (15, 16) is the *proposed n*-diamond (or fcc carbon) modification of diamond; see (31, 32). No *n* diamond was observed in any of our specimens.

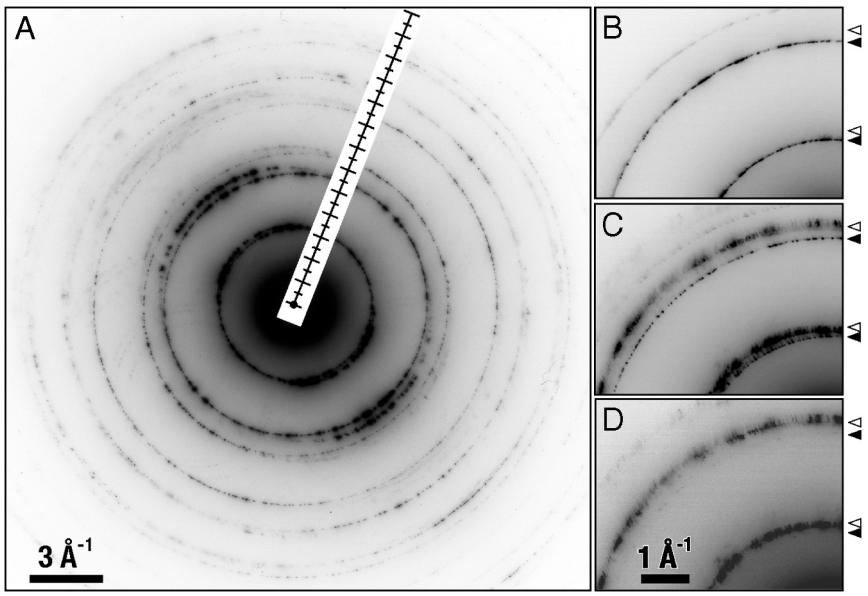

Fig. 4. Typical electron diffraction pattern from graphene/graphane aggregates exhibits (*A*) asymmetrical electron diffraction rings indicative of texturing (i.e., nonhomogeneous dispersion) of two phases. Different regions within the *same* aggregate exhibit diffraction rings from (*B*) only graphene (solid triangles), (*C*) both graphene and graphane, or (*D*) only graphane (open triangles). To aid in visual clarity, the diffraction patterns are displayed in reverse contrast.

In the YD Arlington specimen, we identified an aggregate of nanocrystalline Cu, and in several of our specimens we identified nanocrystalline Cu_2O. These minerals can be misidentified as several of the proposed polytypes/modifications of diamond. Copper (space group 225, $a = 3.6149$ Å) has the same diffraction lines as *n* diamond with planar spacings (i.e., Cu {111} at 2.087 Å) differing by <1.7% from diamond. Further, Cu nanocrystals mounted on standard a-C coated Cu TEM grids can be misidentified as pure C by TEM energy dispersive X-ray spectroscopy. Copper oxide, Cu_2O (space group 201, $a = 4.267$), has diffraction lines very similar to those of the *proposed i*-carbon modified diamond structure [occasionally reported synthesized along with *n* diamond (31)].

Although diffraction lines of 2H hexagonal diamond are distinctly different from those of the major carbonaceous phases identified in YD-boundary carbons (see Table 1), previous researchers (16) misidentified graphene/graphane aggregates as 2H hexagonal diamond in YD black mats. Diffraction patterns reported as 2H diamond by Kennett et al. (16) are clearly missing many relatively intense 2H diamond reflections, e.g., the (101) and (102) (18–20). Furthermore, close inspection of those patterns reveals asymmetric doubled diffraction lines that match closely to those of graphene/graphane aggregates and are inconsistent with 2H diamond (Fig. 3).

Conclusion

Our work emphasizes that rigorous analysis of electron diffraction patterns must be performed together with appropriate elemental quantification or other supplemental structural analysis (e.g., EELS or Raman spectroscopy) for the proper identification of diamond polytypes in carbonaceous materials. Unfortunately, many TEM studies of reported nanometer- to submicrometer-sized diamond polytypes in the literature do not perform such a definitive microanalysis. We demonstrate that previous studies of YD-boundary sediments (15, 16) clearly misidentified graphene/graphane aggregates, shown here to be ubiquitous in several types of carbon-rich materials from sediments (dated from before the YD to the present), as 2H diamond and may have misidentified graphene as cubic diamond. Importantly, we observe no nanodiamonds in any Bølling–Ållerod-YD-boundary sediments examined in this study. It is possible nanodiamonds occur inhomogeneously and only in some of the YD-boundary carbons and hence are not observed in our study. However, Kennett et al. (16) state that "lonsdaleite crystals at Arlington co-occur with carbon spherules and other diamond polymorphs…" and describe the occurrence of nanodiamonds in carbon spherules with "…a TEM study revealed conspicuous subrounded, spherical, and octahedral crystalline particles (2-300 nm) distributed in their carbonaceous matrices…. Analysis of the particles by electron diffraction shows reflections consistent with cubic diamonds…."

The usefulness of cubic nanodiamonds as impact markers in sediments remains unclear because processes other than impact might account for them. Diffraction, supported by EELS and Raman spectroscopy, identified submicrometer (and perhaps nanometer-sized) cubic diamond in an indeterminate population of carbon spherules isolated in upper soils from various sites in Germany and Belgium (33). No links to impact structures have been established, and the origins of these diamonds remain unclear. The reported presence of 2H hexagonal diamond in Bølling–Ållerod-YD-boundary sediments (16) represented the strongest evidence suggesting possible shock processing and an YD impact event. However, we demonstrate that nondiamond carbonaceous minerals were misidentified as 2H diamond in the previous study (16). The observation that morphologically similar carbon spherules occur throughout late Pleistocene to modern sediments (27) together with our results that YD-boundary carbons lack diamonds (particularly the 2H polytype) and are mineralogically similar to older as well as modern spherules casts significant doubt upon the YD impact hypothesis.

Materials and Methods

Microcharcoal aggregates (<63 μm size separate) were isolated from the base of black mat sediment layer at the same locality and stratum (Murray Springs, AZ) reported to contain cubic nanodiamonds (15). Although we did not carbon-date our Murray Springs specimen, Haynes et al. (34) have obtained consistent dates for the base of the black mat throughout the Murray Springs site of 10,260 ± 430 B.P. (calibrated: 11,358–12,546 cal yr B.P., 1σ range), 11,000 ± 100 B.P. (calibrated: 12,737–13,061 cal yr B.P., 1σ range), 10,410± 190 B.P. (calibrated: 12,005–12,559 cal yr B.P., 1σ range), respectively. Therefore, we assume that our specimen dates to be of the same range and are representative of the Bølling–Ållerod-YD boundary. Carbon spherules were isolated from the same locality (Arlington Canyon, Santa Rosa Island, CA) reported to contain hexagonal nanodiamonds (16). Kennett et al. (14, 16) dated the entire basal 5 m of the Arlington YD sequence within the 1σ range 13,100–12,830 cal yr B.P. and reported nanodiamonds in the deepest meter-thick layer (16). In contrast, we obtained calibrated radiocarbon dates spanning >5,000 years over that same 5-m sequence. From that sequence, we examined two specimens for nanodiamonds (from the lowest meter) dating to 12,766–13,044 and 13,379–13,560 cal yr B.P. (1σ range). On neighboring Santa Cruz Island, carbon spherules and glassy carbon were collected from Bølling–Ållerod sediments dated at 15,498–16,209 cal yr B.P. (1σ range) in Sauces Canyon. Our radiocarbon ^{14}C dates were analyzed by the University of California at Irvine Accelerator Mass Spectrometry lab and were calibrated using *Calib* v6.0 calibration software (35, 36); see Table 2. Charred fungal sclerotia were collected from a modern (2006) low-intensity fire at Thursley Bog in Surrey, southern England, and were strikingly similar in morphological form to Pleistocene- as well as Holocene-age carbon spherules (27). All carbonaceous grains were extracted from the collected sediments using a combination of dilute (10%) hydrogen peroxide to break down the clays, followed by digestion in hydrofluoric acid; for further details, see ref. 27.

Several particles (i.e., carbon spherules, microcharcoal, or glassy carbon aggregates) from each specimen were crushed between quartz disks (without solvent), and the fine powder was mounted directly on holey a-C film-coated TEM grids by gently placing the TEM support film in physical contact with the powder. Between 262 and 545 submicrometer-sized particles per TEM mount (2,200 particles total) were individually characterized by TEM selected-area electron diffraction to identify their structure. Elemental and supplemental structural analysis of representative grains from the different structural types was performed using EELS. Specimens were analyzed using a 200-kV JEOL JEM-2100F field emission scanning transmission electron microscope (at Washington University), equipped with high-resolution pole piece and a Schottky field emission gun. The instrument is equipped with a Gatan Tridiem imaging filter capable of performing EELS, EELS spectrum imaging, and electron energy-fil-

Table 2. ^{14}C radiocarbon and calibrated ages

Laboratory/ specimen number	Height (m above datum)	Material dated	^{14}C age, yr	Calibrated age, cal yr B.P.: median*	Calibrated age, cal yr BP: 1-sigma*	Calibrated age, cal yr BP: 2-sigma*
Santa Cruz Island Sauces Canyon						
UCIAMS 46051/SCI-07-P4	3.37	Organics from centrifuge	13,080 ± 30	15,818	15,498–16,209	15,221–16,402
Santa Rosa Island Middle Arlington Canyon						
UCIAMS 66950/SRI-09028	Near basal	Charred wood	11,020 ± 25	12,890	12,766–13,044	12,718–13,079
UCIAMS 66951/SRI-09-29c	Near basal	Charcoal	11,625 ± 25	13,456	13,379–13,560	13,341–13,619

*Calibrated using *Calib* v6.0 Radiocarbon Calibration software (35, 36).

tered imaging. EELS spectra were collected in the diffraction mode of the transmission electron microscope (i.e., image coupling to the EELS spectrometer) and were corrected for dark current and channel-to-channel gain variation of the CCD detector array. To quantify elemental compositions, EELS partial cross-sections were calculated from Hartree–Slater models.

ACKNOWLEDGMENTS. We thank T. J. Bernatowicz and K. Croat for presolar graphite specimens as well as valuable discussions. This work was partially funded by the Center for Materials Innovation at Washington University, National Geographic Society, National Science Foundation (EAR-0746015), and the Royal Holloway strategy fund.

1. Björck S, et al. (1996) Synchronized terrestrial-atmospheric deglacial records around the North Atlantic. *Science* 274:1155–1160.
2. Alley RB, et al. (1993) Abrupt increase in Greenland snow accumulation at the end of the Younger Dryas event. *Nature* 362:527–529.
3. Alley RB, Clark PU (1999) The deglaciation of the Northern Hemisphere: A global perspective. *Annu Rev Earth Planet Sci* 27:149–182.
4. Broecker WS (2003) Does the trigger for abrupt climate change reside in the ocean or in the atmosphere? *Science* 300:1519–1522.
5. Muscheler R, et al. (2008) Tree rings and ice cores reveal ^{14}C calibration uncertainties during the Younger Dryas. *Nat Geosci* 1:263–267.
6. Severinghaus JP, Sowers T, Brook EJ, Alley RB, Bender ML (1998) Timing of abrupt climate changes at the end of the Younger Dryas interval from thermally fractionated gases in polar ice. *Nature* 391:141–146.
7. Grayson DK (2007) Deciphering North American Pleistocene extinctions. *J Anthropol Res* 63:185–213.
8. Faith JT, Surovell TA (2009) Synchronous extinction of North America's Pleistocene mammals. *Proc Natl Acad Sci USA* 106:20641–20645.
9. Haynes CV, Jr (2008) Younger Dryas "black mats" and the Rancholabrean termination in North America. *Proc Natl Acad Sci USA* 105:6520–6525.
10. Buchanan B, Collard M, Edinborough K (2008) Paleoindian demography and the extraterrestrial impact hypothesis. *Proc Natl Acad Sci USA* 105:11651–11654.
11. Teller JT, Leverington DW, Mann JD (2002) Freshwater outbursts to the oceans from glacial Lake Agassiz and their role in climate change during the last deglaciation. *Quaternary Sci Rev* 21:879–887.
12. Clement AC, Cane MA, Seager R (2001) An orbitally driven tropical source for abrupt climate change. *J Climate* 14:2369–2375.
13. Firestone RB, et al. (2007) Evidence for an extraterrestrial impact 12,900 years ago that contributed to the megafaunal extinctions and the Younger Dryas cooling. *Proc Natl Acad Sci USA* 104:16016–16021.
14. Kennett DJ, et al. (2008) Wildfire and abrupt ecosystem disruption on California's Northern Channel Islands at the Ållerød–Younger Dryas boundary (13.0–12.9 ka). *Quaternary Sci Rev* 27:2530–2545.
15. Kennett DJ, et al. (2009) Nanodiamonds in the Younger Dryas boundary sediment layer. *Science* 323:94.
16. Kennett DJ, et al. (2009) Shock-synthesized hexagonal diamonds in Younger Dryas boundary sediments. *Proc Natl Acad Sci USA* 106:12623–12628.
17. Quade J, Forester RM, Pratt WL, Carter C (1998) Black mats, spring-fed streams, and late-glacial-age recharge in the Southern Great Basin. *Quaternary Res* 49:129–148.
18. Bundy FP, Kasper JS (1967) Hexagonal diamond—A new form of carbon. *J Chem Phys* 46:3437–3446.
19. Hanneman RE, Strong HM, Bundy FP (1967) Hexagonal diamonds in meteorites: Implications. *Science* 155:995–997.
20. Frondel C, Marvin UB (1967) Lonsdaleite, a hexagonal polymorph of diamond. *Nature* 214:587–589.
21. Erlich EI, Hausel WD (2002) *Diamond Deposits: Origin, Exploration, and History of Discovery* (Society for Mining, Metallurgy, and Exploration, Littleton, CO).
22. Marlon JR, et al. (2009) Wildfire response to abrupt climate change in North America. *Proc Natl Acad Sci USA* 106:2519–2524.
23. Paquay FS, et al. (2009) Absence of geochemical evidence for an impact event at the Bølling–Allerød/Younger Dryas transition. *Proc Natl Acad Sci USA* 106:21505–21510.
24. Surovell TA, et al. (2009) An independent evaluation of the Younger Dryas extraterrestrial impact hypothesis. *Proc Natl Acad Sci USA* 106:18155–18158.
25. Kaiser K, et al. (2009) Palaeopedological marker horizons in northern central Europe: Characteristics of Lateglacial Usselo and Finow soils. *Boreas* 38:591–609.
26. Haynes CV, Jr, et al. (2010) The Murray Springs Clovis site, Pleistocene extinction, and the question of extraterrestrial impact. *Proc Natl Acad Sci USA* 107:4010–4015.
27. Scott AC, et al. (2010) Fungus, not comet or catastrophe, accounts for carbonaceous spherules in the Younger Dryas 'impact layer'. *Geophys Res Lett* 37:L14302, 10.1029/2010GL043345.
28. Geim AK, Novoselov KS (2007) The rise of graphene. *Nat Mater* 6:183–191.
29. Elias DC, et al. (2009) Control of graphene's properties by reversible hydrogenation: Evidence for graphane. *Science* 323:610–613.
30. Bernatowicz TJ, et al. (1996) Constraints on stellar grain formation from presolar graphite in the Murchison Meteorite. *Astrophys J* 472:760–782.
31. Yamada K, Sawaoka AB (1994) Very small spherical crystals of distorted diamond found in a detonation product of explosive/graphite mixtures and their formation mechanism. *Carbon* 32:665–673.
32. Konyashin I, et al. (2006) A new hard allotropic form of carbon: Dream or reality? *Int J Refract Met H* 24:17–23.
33. Yang ZQ, et al. (2008) TEM and Raman characterisation of diamond micro- and nanostructures in carbon spherules from upper soils. *Diam Relat Mater* 17:937–943.
34. Haynes CV, Jr (2007) *Murray Springs: A Clovis Site with Multiple Activity Areas in the San Pedro Valley, Arizona*, eds CV Haynes, Jr and BB Huckell (Univ Arizona Press, Tucson), pp 229–239.
35. Stuiver M, Reimer PJ (1993) Extended ^{14}C data base and revised CALIB 3.0 ^{14}C age calibration program. *Radiocarbon* 35:215–230.
36. Reimer PJ, et al. (2009) INTCAL09 and MARINE09 radiocarbon age calibration curves, 0–50,000 years cal BP. *Radiocarbon* 51:1111–1150.